Journal of Food Science

ORIGINAL ARTICLE OPEN ACCESS

Health, Nutrition, and Food

Investigation of the Antioxidant, Antibiofilm, and Endocrine-disrupting Potential of *Amaranthus retroflexus* Methanol Extract Used as Food: Network and Molecular Docking Analyses

Mehmet Aytar[1] | Emine İncilay Torunoğlu[2] | Erdi Can Aytar[3] | Alper Durmaz[4] | Betül Aydın[5] | Abidin Gümrükçüoğlu[6]

[1]Institute of Science, Aydın Adnan Menderes University, Aydın, Türkiye | [2]Department of Medical Biochemistry, Necmettin Erbakan University, Konya, Türkiye | [3]Department of Horticulture, Uşak University, Uşak, Türkiye | [4]Ali Nihat Gökyiğit Botanical Garden Application and Research Center, Artvin Çoruh University, Artvin, Türkiye | [5]Department of Biology, Gazi University, Ankara, Türkiye | [6]Medicinal-Aromatic Plants Application and Research Center, Artvin Çoruh University, Artvin, Türkiye

Correspondence: Erdi Can Aytar (erdicanaytar@gmail.com)

Received: 13 January 2025 | **Revised:** 16 May 2025 | **Accepted:** 23 May 2025

Funding: The authors received no specific funding for this work.

Keywords: *Amaranthus retroflexus* antioxidant activity | antibiofilm activity | molecular docking | network analysis

ABSTRACT: This study aims to investigate the antioxidant and iron chelating activities; phytochemical composition; and profile, antibiofilm activity, in silico molecular docking, and network analysis of the methanol extract of *Amaranthus retroflexus*. The extract showed an IC_{50} value of 3.50 mg/mL in the DPPH assay and 6.61 mg/mL in the iron-chelating assay. The total phenolic and flavonoid contents were determined as 30.54 mg GAE/g DW and 29.28 mg QE/g DW, respectively. Antibiofilm tests revealed 7% inhibition against *Pseudomonas aeruginosa*, while biofilm formation increased by 10% in *Staphylococcus aureus* 25923. HPLC analysis identified key bioactive compounds, including ascorbic acid, gallic acid, vanillic acid, rosmarinic acid, oleuropein, rutin, and quercetin. Macroelement analysis indicated high potassium and magnesium levels, highlighting the plant's nutritional potential. In the in silico endocrine-disrupting analysis, compounds such as ascorbic acid, vanillic acid, and quercetin exhibited a low-risk profile, while rosmarinic acid, gallic acid, and baicalin demonstrated moderate binding potential with specific receptors. Molecular docking studies demonstrate that oleuropein, rutin, and baicalin exhibit strong binding affinity with target proteins. Network analysis has identified key biological pathways related to inflammation, oxidative stress, and immune modulation, highlighting the roles of rutin and oleuropein in managing *P. aeruginosa* infections. Following the network analysis, molecular docking studies reveal that oleuropein and rutin have an even stronger binding affinity with target proteins.

Practical Application

The findings of this study suggest that *Amaranthus retroflexus* extract may serve as a natural source of antioxidant and iron-chelating agents, as well as bioactive compounds with potential roles in managing bacterial biofilm formation. Due to its phytochemical richness and essential mineral content, the extract could be further explored in the development of plant-based supplements, functional foods, or natural preservatives. This research provides a foundation for future studies focused on safe and sustainable health-supporting products.

1 | Introduction

Amaranthus retroflexus L., a species that belongs to the Amaranthaceae family, is more commonly known as redroot pigweed *retroflexus* (Davis 1967). This weed is widely distributed in temperate and subtropical regions, exhibiting significant agricultural, ecological, and pharmacological consequences (Kumar 2024; POWO 2024a, 2024b). Notwithstanding its reputed classification as a weed, recent studies have redirected their focus toward the potential bioactive properties of the subject (Caselato-Sousa and Amaya-Farfán 2012). Indeed, the presence of secondary metabolites such as flavonoids, phenolic acids, and betacyanins has been identified as contributing to the antioxidation, antimicrobial, and anti-inflammatory activities attributed to the subject (Fiorito et al. 2017; Singhania et al. 2024). The species is also notable for its high nutritional content, which is characterized by a significant presence of proteins, dietary fiber, essential minerals, and vitamins (Nazeer and Firincioglu 2022; Sărăcin et al. 2023; Singhania et al. 2024). The consumption of the plant is traditional in several different cultures, including those in India, Mexico, and among Native American populations (Elias and Dykema 2009). However, it should be noted that it may be toxic to livestock if consumed in excess (Fiorito et al. 2017).

Phytochemical analyses of *Amaranthus* species have yielded several compounds, including rutin, quercetin, and oleuropein, which have been shown to possess free radical scavenging activity, the capacity to inhibit biofilm formation, and the potential to modulate immune responses (Sărăcin et al. 2023; Almuhanna et al. 2024). These bioactivities indicate their potential to control infections caused by opportunistic pathogens such as *Pseudomonas aeruginosa*. These are characterized by the formation of resilient biofilms and are associated with chronic and device-related infections (Tuon et al. 2022).

Notwithstanding the mounting acknowledgment of *A. retroflexus* as a prospective reservoir of natural antioxidants and antimicrobial agents, studies that comprehensively evaluate its biological properties, encompassing antioxidant, antibiofilm, and molecular interactions, remain sparse. Furthermore, there is limited knowledge concerning the molecular mechanisms through which its primary phytochemicals interact with bacterial virulence pathways and host immune regulators.

The present study has been conducted for the purpose of evaluating the antioxidant activity, antibiofilm potential, phytochemical composition, and endocrine-disrupting properties of the methanolic extract of *A. retroflexus* aboveground parts. Furthermore, in silico methods, namely molecular docking and network analysis, were employed to assess the interactions of the key compounds with target proteins relevant to *P. aeruginosa* pathogenicity and host immune signaling. These findings may provide a scientific basis for the potential use of *A. retroflexus* in food and pharmaceutical applications.

2 | Materials and Methods

2.1 | Collection and Preparation of *A. retroflexus* Plant Material

A. retroflexus materials were collected on August 13, 2023, from rural areas in the Gölardı region of the Terme district, Samsun Province. The collected specimens were identified by Dr. Alper Durmaz and registered in the Herbarium of the Department of Biology, Faculty of Science, Ondokuz Mayıs University, under the herbarium number OMUB-6615.

The aboveground parts of *A. retroflexus* were dried in an oven at 40°C for 72 h. The dried plant material was then mixed with methanol at a ratio of 1:10 (plant [100 g]/methanol solvent [1000 mL]) and left to macerate in a dark environment at room temperature for 2 days. Following the extraction, the methanol solution was filtered through Whatman No. 1 filter paper (Whatman International Ltd., Maidstone, UK) Whatman No. 1 filter paper (pore size ~11 μm) was used to remove particulate matter; this filter does not possess a defined molecular weight cutoff. The solvent was then evaporated under reduced pressure using a rotary evaporator at 40°C. The resulting solid extracts were stored at 4°C for further analysis (Aytar 2024). The solid-to-solvent ratio of 1:10 (w/v) was selected based on preliminary optimization trials and literature reports indicating its efficiency in extracting phenolic compounds from similar plant matrices. This ratio was found to provide sufficient extraction yield while ensuring practical solvent usage (Insuan et al. 2022; Aytar et al. 2025).

2.2 | Phytochemical Studies

2.2.1 | Total Phenolic Content

Folin–Ciocalteu reagent method was used. Plant extracts were diluted to a concentration of 1 mg/mL. Note that 0.5 mL was taken from these solutions and mixed with 2.5 mL of Folin–Ciocalteu reagent and 2 mL of 7.5% $NaHCO_3$. The Folin–Ciocalteu reagent had been previously diluted 10-fold with water. The mixture was incubated at 45°C for 15 min. After incubation, the absorbance of the reaction mixture was measured at 765 nm using a UV spectrophotometer (Epoch; Bio-Tek, Winooski, VT, USA). A calibration curve was prepared. Each experiment was performed in triplicate. The results were expressed as mg gallic acid equivalents (GAE) per gram of extract dry weight (DW)(Singleton et al. 1999).

2.2.2 | Total Flavonoid Content

The total flavonoid content was measured using a spectrophotometric method. The procedure is as follows: Extracts from each plant material (1 mL containing 0.1 mg/mL) were diluted with water (4 mL) in a 10 mL volumetric flask. Initially, 5% $NaNO_2$ solution (0.3 mL) was added to each flask. At the fifth minute, 10% $AlCl_3$ solution (0.3 mL) was added. At the sixth minute, 1.0 M NaOH (2 mL) was added. Then, water (2.4 mL) was added to the

reaction flask and mixed well. The absorbance of the reaction mixture was measured at 510 nm using a UV spectrophotometer (Epoch; Bio-Tek, Winooski, VT, USA). A calibration curve was prepared. Each experiment was performed in triplicate. The results were expressed as mg quercetin equivalents (QE) per gram of extract DW (Dewanto et al. 2002).

2.3 | Antioxidant Activity of *A. retroflexus* Extract

2.3.1 | Diphenyl-1-picrylhydrazyl (DPPH) Assay

The DPPH test technique was used (Aytar 2024). *A. retroflexus* extract was prepared at different concentrations (1, 0.5, 0.25, 0.125, 0.0625, 0.03125 mg/mL). A DPPH methanol solution was prepared at 80 μg/mL. Note that 2 mL of the DPPH solution was added to each extract solution, and the mixtures were vortexed. The reaction mixtures were incubated at 27°C for 30 min. At the end of the incubation period, the absorbance of the reaction mixtures was measured at 517 nm using UV spectrophotometry (Epoch; Bio-Tek, Winooski, VT, USA). BHT was used as the standard control. BHT stock solution was prepared at different concentrations (500, 250, 125, 62.5, 32.25, 16.125 μg/mL). All measurements were performed in triplicate. A calibration curve was prepared. The IC_{50} values of the extracts and ethylenediaminetetraacetic acid (EDTA) were calculated. The antioxidant activity of the *A. retroflexus* extract was evaluated using the following formula:

$$\text{DPPHscavengingactivity (\%inhibition)} = [(A_{\text{control}} - A_{\text{sample}})/A_{\text{control}}] \times 100.$$

2.3.2 | Determination of Ferrous Ion Chelating Capacity

Ferrous ion chelating capacity was measured using a spectrophotometric method. The extract of *A. retroflexus* was prepared in different concentrations (1, 0.5, 0.25, 0.125, 0.0625, 0.03125 mg/mL). 1.6 mL of the extract, 2.16 mL of distilled water, and 80 μL of 2 mM $FeCl_2$ were mixed in a test tube. The reaction was initiated by adding 160 μL of 5 mM ferrozine. The solutions were thoroughly mixed and allowed to stand at room temperature (25°C) for 10 min. After incubation, the absorbance of the reaction mixtures was measured at 562 nm using UV spectroscopy (Epoch; Bio-Tek, Winooski, VT, USA). EDTA was used as the standard control. The EDTA stock solution was prepared at 500 μg/mL and serially diluted by half to obtain six different concentrations. IC_{50} values were calculated, and a calibration curve was constructed. All measurements were performed in triplicate. The ferrous ion chelating ability was calculated using the following formula (Dinis et al. 1994).

The antioxidant activity of the *A. retroflexus* extract was evaluated using the following formula:

$$\text{Ferrousionchelatingcapacity (\%inhibition)} = [(A_{\text{control}} - A_{\text{sample}})/A_{\text{control}}] \times 100.$$

2.4 | Antibiofilm Activity

Antibiofilm properties of *A. retroflexus* methanol extracts were investigated on biofilm-forming bacteria *P. aeruginosa* PAO1 (ATCC 15692) and *Staphylococcus aureus* ATCC 25923. The biofilm formation of bacterial strains was performed with 96-well microplates. For this process, overnight cultures were diluted at a 1:100 ratio with a TSB liquid medium containing 1% glucose. A final volume of 200 μL was added to each well from these diluted cultures. Different concentrations of *A. retroflexus* methanol extracts were added to the wells to achieve final concentrations of 0.5 and 1 mg/mL. The control group used bacterial cultures without plant extracts, while the negative control wells contained only the culture medium. The plates were incubated at 37°C for 24 h without shaking to allow biofilm formation. After incubation, unattached bacteria were removed by washing three times with distilled water. The attached bacteria were then fixed by drying at 60°C for 1 h (Stepanović et al. 2007). The amount of biofilm formed was measured spectrophotometrically at a wavelength of 595 nm (Li et al. 2014). All experiments were repeated three times.

The formula calculated the reduction in biofilm formation:

$$\text{Antibiofilm activity } (\%) = (1 - \text{OD sample}/\text{OD control}).$$

2.5 | Chemical Profile

2.5.1 | HPLC-DAD Analysis

A dry powder sample (1 g) was extracted using 10 mL of methanol. The extraction process began with ultrasonication using a Fisher brand FB15054 ultrasonicator for 30 min to enhance the release of target compounds into the solvent. Following this step, the mixture was transferred to a Heidolph Unimax 1010 orbital shaker and incubated in darkness at room temperature (25°C) for 24 h, allowing efficient extraction under controlled conditions. After incubation, the extracts were filtered through Whatman no 1 filter paper (Whatman International Ltd., Maidstone, UK) to remove larger particles. The filtrate was then further purified using a 0.45-μm syringe filter to ensure the removal of finer particulates, resulting in a clear and purified extract ready for analysis. Analytical procedures for quantifying ascorbic acid, gallic acid, 3,4-hydroxybenzoic acid, catechin, epicatechin, caffeic acid, vanillic acid, rutin, coumaric acid, ferulic acid, rosmarinic acid, myricetin, quercetin, and apigenin were performed on an ACE 5 C18 column (250 mm × 4.6 mm, 5 μm). The mobile phase consisted of acetonitrile (A) and 1.5% acetic acid solution (B), with a gradient program starting at 15% A:85% B and progressing to 40% A:60% B over 29 min. The instrumental setup included a 1260 DAD WR detector monitoring at wavelengths of 250, 270, and 320 nm, a 1260 Quaternary Pump operating at 0.7 mL/min, a 1260 Vial Sampler with 10 μL injection volume, and a G7116A column compartment maintained at 35°C.

For pyrogallol, chlorogenic acid, syringic acid, cyanidin chloride, resveratrol, oleuropein, hesperetin, kaempferol, baicalein, and chrysin analyses, identical column specifications were employed, while utilizing methanol (A) and 1.5% acetic acid solution (B) as the mobile phase. The gradient program followed a multistage profile: initially 10% A:90% B, transitioning to 40% A:60% B by

29 min, then to 60% A:40% B by 40 min, and finally reaching 90% A:10% B from 40 to 53 min. The instrumentation was configured with a 1260 DAD WR detector operating at wavelengths of 280, 290, 320, 370, and 535 nm, a 1260 Quaternary Pump at 0.7 mL/min, a 1260 Vial Sampler delivering 10 µL injections, and a G7116A column oven set at 35°C. The quantification of phenolic compounds was achieved using calibration curves constructed with six standard concentrations (25, 50, 75, 100, 200, and 300 µg/mL). The extracted samples were analyzed using HPLC-DAD, ensuring precise identification and quantification. Combining ultrasonication, extended incubation, dual-stage filtration, and chromatographic separation, this method maximized compound recovery and delivered reliable analytical results (Gümrükçüoğlu et al. 2020).

The seven bioactive compounds presented in Table 2 include all compounds that were detected and quantified in our high-performance liquid chromatography (HPLC) analysis. Our methodology examined one vitamin, 12 phenolic compounds, and 11 flavonoids; however, only the compounds shown in the table were detected above the quantification limit. The other standard compounds analyzed were either not detected or remained below the quantification limit. The compounds in Table 2 are not selected main compounds, but rather all compounds that could be analytically identified.

2.5.2 | ICP-MS Analysis for Metal Ion Quantification

A. retroflexus plant samples were prepared in ground and dried form for analysis. A specified amount of plant material (0.30–0.80 g, ±0.0001 g precision) was transferred into Teflon vessels, followed by the addition of 6–10 mL of concentrated ultrapure nitric acid (67%–68%) and 0–1 mL of ultrapure water. These Teflon vessels were then placed in an Anton Paar Multiwave 5000 Microwave Reaction System, which operated under the following conditions: heating to 180°C for 20 min, maintaining a constant temperature for 10 min, and cooling to 70°C for 20 min. The resulting solutions were filtered through a 0.45 µM syringe filter to obtain clear solutions. These filtered solutions were transferred into 50 mL volumetric flasks and diluted to the mark with a 2% nitric acid–ultrapure water mixture. Standard solutions for metal ions (Mg, K, Ca, C, and H) were prepared using stock aqueous solutions at 1000 mg/L concentrations. Appropriate dilutions prepared working solutions in the concentration range of 0–500 µg/L in a total volume of 50 mL. These solutions were analyzed in triplicate using the ICP-MS (Agilent 7900 model inductively coupled plasma mass spectrometry) instrument, and a calibration curve was constructed. The calibration curve was optimized to achieve an R^2 value between 1.00 and 0.99, and measurements were performed accordingly. The run conditions of the ICP-MS were as follows: plasma flow (15 L/min), auxiliary flow (0.9 L/min), nebulizer flow (1.0 L/min), nebulizer pump (0.3 rps), argon as plasma gas, makeup gas (1.0 L/min), and rinse time (45 s).

2.5.3 | Determination of Elemental Analysis

The elemental analysis of C, H, N, and S was conducted using a CHNS-O analyzer (Flash 2000, Thermo Scientific). The material was processed into a uniform powder using an electric grinder equipped with a stainless steel tank. For analysis, approximately 10 mg of each sample was placed in tin capsules and subjected to combustion with an oxygen flow rate of 140 mL/min at a furnace temperature of 950°C. The gases produced during combustion (CO_2, H_2O, and N_2) were separated utilizing a constant helium carrier gas flow of 100 mL/min with the oven temperature maintained at 65°C. The results are presented as percentages.

2.6 | Assessment of Endocrine Disruptor Potential

The potential of metabolites to bind to 15 distinct nuclear receptors was evaluated using the Endocrine Disruptome platform (http://endocrinedisruptome.ki.si/). This platform simulates interactions by virtually docking each metabolite with crystal structures of several nuclear receptors, such as the androgen receptor (AR), estrogen receptors α and β (ER α/β), glucocorticoid receptor (GR), liver X receptors α and β (LXR α/β), mineralocorticoid receptor (MR), peroxisome proliferator-activated receptors α, β, and γ (PPAR α, PPAR β, and PPAR γ), progesterone receptor (PR), retinoid X receptor α (RXR α), and thyroid receptors α and β (TR α and TR β). The server categorizes the results into three risk levels: red indicates a high binding potential, orange and yellow indicate moderate binding potential, and green represents a low likelihood of interaction with the receptors.

2.7 | Molecular Docking Studies

The 3D structure of *P. aeruginosa* antitoxin HigA with pa2440 promoter (PDB ID: 7CSW), crystal structure of recombinant human acetylcholinesterase (AChE) in complex with donepezil (PDB ID: 4EY7) and cytokine receptor complex (PDB ID: 2B5I) was retrieved from the Protein Data Bank (https://www.rcsb.org/). Water molecules and cofactors were initially excluded, and hydrogen atoms were added using AutoDockTools (ADT). The 3D models of natural product compounds were downloaded in SDF format from PubChem and converted to PDB format using Discovery Studio Visualizer for subsequent docking simulations. Before performing docking, the grid center for each protein target was determined using the AutoGrid program in AutoDockTools. The grid size was set to 40 points per dimension, with a spacing of 0.375 Å across all simulations. Molecular docking was conducted using AutoDock Vina (Trott and Olson 2010) to calculate the binding affinities of each ligand with the target protein. The number of output poses (modes) was set to 10, and the energy range was adjusted to 9 kcal/mol. To improve the accuracy of the docking results, the exhaustiveness parameter was set to 1000.2D and 3D visuals are demonstrated by BIOVIA Discovery Studio Visualizer software (Biovia 2021).

2.8 | Target-Pathway Interaction Network Construction

Gene clusters were analyzed using the Enrichr platform to evaluate the relationship with *P. aeruginosa*. Genes were entered into the input field, and disease-related data, including DisGeNet and OMIM, were downloaded. Protein–protein interaction (PPI) networks were constructed using intersecting targets in the STRING

TABLE 1 | Results of antioxidant and iron chelation assays, and total phenolic and flavonoid contents of *A. retroflexus* and standards (mean ± SD; $n = 3$).

	DPPH assay (IC_{50} mg/mL)	Iron chelation assay (IC_{50} mg/mL)	Total phenolic content (mg GAE/g extract DW)	Total flavonoid content (mg QE/g extract DW)
Amaranthus retroflexus	3.50 ± 0.09	6.61 ± 0.64	30.54 ± 1.06	29.28 ± 2.14
BHT	0.23 ± 0.01	—	—	—
EDTA	—	5.30 ± 4.44	—	—

11.5 database, with the species set to "Homo sapiens" and a confidence threshold of >0.4. Unlinked targets were excluded, and the resulting networks were visualized and analyzed in Cytoscape (version 3.10.1), where nodes represented key targets and edges indicated their interactions. Additionally, targets associated with plants and *P. aeruginosa* were integrated to construct a drug–component–target–disease network in Cytoscape, with nodes representing targets and edges illustrating potential relationships. Pathway enrichment analysis was performed using the Enrichr database to explore the mechanisms of plants in addressing *P. aeruginosa*–related conditions, focusing on KEGG and Reactome pathways. Critical proteins and pathways identified through this analysis were used to develop a target-pathway interaction network in Cytoscape, providing deeper insights into the underlying biological mechanisms.

2.9 | Statistical Analysis

Data are presented as the mean ± SD value, which was computed with Minitab 18 software extended with a statistical package and Microsoft Excel 365.

3 | Results and Discussion

3.1 | Result of Antioxidant Activity and Phytochemical Contents

Table 1 presents the antioxidant and iron chelation assay results and the total phenolic and flavonoid contents of *A. retroflexus*. The *A. retroflexus* extract exhibits strong antioxidant and iron chelation activities and a rich phytochemical composition.

According to Table 1, the smaller the IC_{50} value, the stronger the anti-radical effect of the plant. The *A. retroflexus* extract demonstrated good antioxidant activity with an IC_{50} value of 3.50 ± 0.09 mg/mL in the DPPH assay test. Previous studies reported low antioxidant activity for the *A. retroflexus* extract (IC_{50} value 92.7 mg/mL) (Pacifico et al. 2008). Similar results were reported for the methanol extracts of *Amaranthus lividus* and *Amaranthus blitum* leaves (Sarker et al. 2020; Sarker and Oba 2020a). Methanol extracts of *Amaranthus spinosus*, *Amaranthus dubius*, *Amaranthus viridis*, and *Amaranthus tricolor* exhibited good antioxidant activity, ranging from 63.94 ± 3.72 to 92.20 ± 4.21 μg/mL (House et al. 2020), and these results are consistent with the findings of our study. The IC_{50} values for the methanol extract of *A. viridis*, the methanol leaf extract of *A. spinosus*, and the ethyl acetate extract of *A. spinosus* were found to be 53.68, 83.5, and 47.23 μg/mL, respectively (Bulbul et al. 2011; Amabye 2016; Kumari et al. 2018). These values are lower than the IC_{50} value of our extract (IC_{50} = 3.50 mg/mL), indicating that our extract exhibits stronger antioxidant activity.

The excessive accumulation of free iron ions can lead to increased oxidative stress, whereas iron chelating compounds bind these ions, thereby preventing these negative effects and exhibiting antioxidant properties. The *A. retroflexus* extract demonstrated good antioxidant activity with an IC_{50} value of 6.61 ± 0.64 mg/mL in the iron chelation assay (Table 1). The methanol extract of *A. viridis* was found to have IC_{50} values of 32.1 ± 1.11 μg/mL (Kumari et al. 2018), which are lower than the IC_{50} values of our extract, indicating stronger iron chelation activity.

The total phenol content of *A. retroflexus* extract was determined using the Folin–Ciocalteu reagent. The total phenol content of the extract was found to be 30.54 ± 1.06 mg GAE/g extract DW. This value is lower than the values reported by Bang et al. (2021) for *Amaranthus caudatus* extract (84.1 ± 21.0 mg GAE/g), *Amaranthus cruentus* extract (83.8 ± 28.3 mg GAE/g), and *Amaranthus crispus* extract (117.0 ± 14.1 mg GAE/g). Our value is significantly higher than the total phenol content in *Amaranthus hypochondriacus* leaves, which was found to range from 13.23 ± 0.15 g GAE/g to 29.34 ± 0.12 g GAE/g (Sarker and Oba 2020b). Additionally, the study by Kumari et al. (2018) reported that the total phenol content of *A. viridis* extracts was 16.4 ± 0.45 mg CAT/g, which is lower than our value.

The total flavonoid content of *A. retroflexus* extract is approximately 29.28 ± 2.14 mg QE/g extract DW. This value is higher compared to the *A. viridis* extracts reported by Kumari et al. (2018), which had 5.28 ± 0.33 mg QE/g, and the values reported by Sarker and Oba (2020b). Furthermore, it is significantly higher than the results obtained for *A. hypochondriacus* leaf extracts (106.80 ± 0.29 to 170.97 ± 0.32 RE μg/g). The total flavonoid content of *A. caudatus*, *A. crispus*, and *A. cruentus* extracts, as reported by Bang et al. (2021), is 34.9 ± 6.8, 40.4 ± 4.2, and 37.1 ± 7.5 mg QE/g, respectively, which are higher than the results of our study. According to the literature, the content of these total phenolic compounds and flavonoids varies depending on the species, season, growing conditions, sample preparation methods, and the analysis techniques used.

3.2 | Result of Antibiofilm Activity

In the literature, *Amaranthus* protein isolates have been tested for their antibiofilm activities against the Gram-negative *C.*

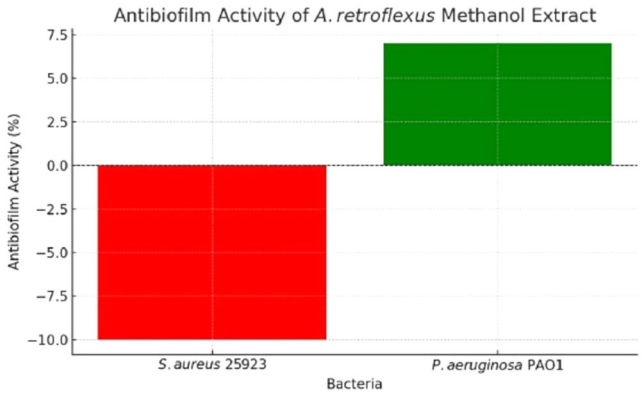

FIGURE 1 | Antibiofilm activity of *A. retroflexus* methanol extract.

albicans (Beema Shafreen et al. 2019). In another study, the betacyanin fraction extracted from *A. dubius* leaves exhibited good antibiofilm activity against *S. aureus*, while the betacyanin fraction from *Hylocereus polyrhizus* demonstrated a stronger antibiofilm effect against *P. aeruginosa* (Yong et al. 2019). The tested *A. retroflexus* extract showed antibiofilm activity against *P. aeruginosa*, but increased biofilm formation in a dose-dependent manner for *S. aureus*. The *N*-acetyl-D-galactosamine-binding lectin extracted from *Amaranthus gangeticus* seeds showed biofilm inhibition against *Escherichia coli* at concentrations of 250, 500, and 1000 μg/mL, with inhibition rates of 37.14%, 65.71%, and 82.85%, respectively (Hasan et al. 2021). In comparison, the *A. retroflexus* extract showed only 7% antibiofilm activity against *P. aeruginosa*. Furthermore, the *Anabasis articulata* extract effectively inhibited biofilm formation in *P. aeruginosa*, reducing it from 41.18% to 17.65% (Gamal et al. 2022). The *A. retroflexus* methanol extract demonstrated antibiofilm activity against *P. aeruginosa*. The *Curcuma longa* rhizome extract significantly inhibited biofilm formation against *S. aureus* and *P. aeruginosa* isolates (Suwal et al. 2021), whereas the *A. retroflexus* methanol extract inhibited biofilm formation only in *P. aeruginosa* isolates, with a dose-dependent effect on biofilm formation in *S. aureus* (Figure 1).

The methanol extract of *Acacia macrostachya* stem bark reduced biofilm biomass in *S. aureus* and *P. aeruginosa* isolates, demonstrating broad potential against bacterial resistance mechanisms (Barfour et al. 2021). In contrast, the *A. retroflexus* methanol extract reduced biofilm formation only in *P. aeruginosa* isolates, while a dose-dependent increase in biofilm formation was observed for *S. aureus*. This suggests that the *A. macrostachya* extract may have a broader antibiofilm effect. The aqueous extract of *Acacia nilotica* reduced biofilm activity in *P. aeruginosa* (Elamary et al. 2020). In comparison, the *A. retroflexus* methanol extract reduced biofilm activity only in *P. aeruginosa*. The acetone extract of *Acca sellowiana* fruit reduced biofilm biomass in *S. aureus* by inhibiting initial attachment without affecting bacterial growth, and disrupted the biofilm structure (Dell'Olmo et al. 2021). In contrast, the *A. retroflexus* methanol extract increased biofilm formation in *S. aureus*. The methanol extract of *Adiantum philippense* inhibited biofilm structure in both *S. aureus* and *P. aeruginosa* (Adnan et al. 2020). The essential oil of *Eucalyptus globulus* leaves and isolated 1,8-cineole inhibited initial attachment, reducing biofilm biomass in *S. aureus* and *P. aeruginosa*, and decreased biofilm viability (Merghni et al., 2018). Similarly, the *A. retroflexus* methanol extract inhibited biofilm formation in P. *aeruginosa* isolates, but increased biofilm formation in *S. aureus* isolates.

3.3 | Result of Phytochemical Content Analysis

The phytochemical components obtained from the HPLC analysis of *A. retroflexus* extract are presented in Table 2. The bioactive compound profile of *A. retroflexus* extract was determined by HPLC analysis. Among the identified compounds, rutin was the most abundant, with a concentration of 777.02 mg/L in the extract, corresponding to approximately 5.29 mg/g in the dry plant material and 288.55 mg/g in the dry extract. Ascorbic acid was detected at 88.12 mg/L, equivalent to about 0.58 mg/g in the dry plant and 32.02 mg/g in the dry extract. Oleuropein was present at 52.56 mg/L, translating to approximately 0.35 mg/g in the dry plant and 19.11 mg/g in the dry extract. Quercetin was quantified at 31.93 mg/L, corresponding to 0.21 and 11.61 mg/g in the dry plant and dry extract, respectively. Gallic acid was found at 18.42 mg/L, equating to approximately 0.12 mg/g in the dry plant and 6.71 mg/g in the dry extract. Rosmarinic acid was measured at 5.19 mg/L, which corresponds to 0.03 mg/g in the dry plant and 1.89 mg/g in the dry extract. Vanillic acid was identified at a lower concentration of 1.76 mg/L, equivalent to approximately 0.01 mg/g in the dry plant and 0.64 mg/g in the dry extract. Finally, baicalin was detected at 2.08 mg/L, corresponding to around 0.01 mg/g in the dry plant material and 0.76 mg/g in the dry extract. These results highlight the rich phenolic and flavonoid composition of *A. retroflexus*, supporting its potential biological activity. However, among the other compounds evaluated within the scope of the analytical method, 3,4-hydroxybenzoic acid, catechin, epicatechin, caffeic acid, coumaric acid, ferulic acid, myricetin, apigenin, pyrogallol, chlorogenic acid, syringic acid, cyanidin chloride, resveratrol, hesperetin, kaempferol, baicalein, and chrysin were not detected in the extract samples. Ascorbic acid (Kırmusaoğlu and Kaşıkçı 2020), gallic acid (Sang et al. 2024), vanillic acid (Qian et al. 2020), rosmarinic acid (Ivanov et al. 2022), oleuropein (Guo et al. 2023), rutin (Almuhanna et al. 2024), and quercetin (Almuhanna et al. 2024) are antibiofilm agents that prevent biofilm formation. The chemical compounds found in *A. retroflexus*, such as ascorbic acid, gallic acid, vanillic acid, rosmarinic acid, oleuropein, rutin, and quercetin, are known for their antibiofilm activities and are believed to inhibit biofilm formation in various bacteria, particularly showing significant antibiofilm effects against *P aeruginosa*. However, despite the presence of these compounds, a dose-dependent increase in biofilm formation has been observed in *S. aureus* isolates. This contradictory result arises from the fact that different bacterial species utilize distinct mechanisms for biofilm formation. It is suggested that *S. aureus* may respond differently to these compounds, especially at higher concentrations, leading to an increase in biofilm production. Additionally, the synergistic or antagonistic interactions among the compounds in *A. retroflexus* could contribute to these varying effects; while some compounds inhibit biofilm formation, others may trigger biofilm production by activating signaling pathways that promote biofilm formation.

Ascorbic acid (Gęgotek and Skrzydlewska 2023), gallic acid (Alfei et al. 2020), vanillic acid(Shabani et al. 2023), rosmarinic acid(Aldoghachi et al. 2021), oleuropein(Wang et al. 2021), rutin,

TABLE 2 | Bioactive compounds in *A. retroflexus* extract measured by HPLC.

No.	Compounds	In the extract (mg/L)	Dry plant (mg/g)	Dry extract (mg/g)
1	Ascorbic acid	88.12	≈0.58	≈32.02
2	Gallic acid	18.42	≈0.12	≈6.71
3	Vanillic acid	1.76	≈0.01	≈0.64
4	Rosmarinic acid	5.19	≈0.03	≈1.89
5	Oleuropein	52.56	≈0.35	≈19.11
6	Rutin	777.02	≈5.29	≈288.55
7	Quercetin	31.93	≈0.21	≈11.61
8	Baicalin	2.08	≈0.01	≈0.76

TABLE 3 | Macroelemental composition and elemental analysis of *A. retroflexus*.

No.	Plant species	Macroelements mg (100 g)$^{-1}$			Elemental analysis (%)	
		Mg	K	Ca	Carbon	Hydrogen
1	*Amaranthus retroflexus*	3813.44 ± 39.94	9283.91 ± 54.25	7587.24 ± 55.23	41.64	6.06

and quercetin (Pandey et al. 2020)exhibit antioxidant activity. These bioactive compounds contribute significantly to the antioxidant potential of *A. retroflexus* extract. The extract of *A. retroflexus*, which contains these compounds, shows substantial antioxidant activity, due to the synergistic effects of these substances. Each of these compounds plays a role in scavenging free radicals, reducing oxidative stress, and potentially providing therapeutic benefits. The presence of these compounds in *A. retroflexus* enhances its ability to neutralize oxidative damage, demonstrating its potential as a source of natural antioxidants.

3.4 | Result of Macroelements and Elemental Analysis

The macroelement composition and elemental analysis of *A. retroflexus* are shown in Table 3. The potassium (K) level in *Amaranthus* spp. has been found to be 508 mg/100 g (Sattar et al. 2024). *Amaranth* seeds contain 159 mg/100 g calcium (Ca), 248 mg/100 g magnesium (Mg), and 508 mg/100 g K (Soriano-García and Aguirre-Díaz 2020). The mineral composition of *A. tricolor* includes 1.7±0.04 g/100 g Ca, 3.7±0.26 g/100 g K, and 2.9±0.01 g/100 g Mg (Shukla et al. 2006). In *Amaranthus* spp., the Ca level has been found to be 267 mg/100 g, and the K level 411 mg/100 g (Rastogi and Shukla 2013). In *A. hybridus* leaves, the K, Ca, and Mg contents were determined to be 8.86, 26.12, and 29.31 mg/100 g, respectively (Sarker et al. 2022). The K, Ca, and Mg contents in *A. retroflexus* are higher compared to those reported in other studies.

Recent studies have shown that Mg, Ca, and K can influence the structural, antimicrobial, and biochemical properties of plant-based materials. For example, calcium contributes to cross-linking within biopolymer structures, enhancing film stability, barrier properties, and microbial resistance (Bankar et al., 2024). Similarly, magnesium plays a key role in energy metabolism and enzymatic activities; in this regard, it may affect the biological interactions and antimicrobial potential of extracts (Nguyen et al. 2018). Potassium, on the other hand, regulates water balance, ion transport, and intracellular signaling pathways, which may indirectly influence the overall biological functionality of plant-based compounds (Ge et al. 2022).

3.5 | Result of Endocrine-Disrupting Potential

The analysis evaluated the binding potential of seven compounds with 15 nuclear receptors, providing valuable insights into their endocrine-disrupting potential. According to the results, most compounds exhibited low binding potential with the receptors, while some demonstrated moderate interactions with specific receptors. It is important to note that the system does not calculate binding interactions for molecules with a molecular weight exceeding 500 g/mol. As a result, compounds such as rutin and oleuropein, which exceed this molecular weight threshold, could not be evaluated for their binding potential in this analysis.

The study specifically assessed the binding potential of ascorbic acid, gallic acid, vanillic acid, rosmarinic acid, quercetin, and baicalin with nuclear receptors (Figures S1–S6). These compounds were categorized based on their binding energies and analyzed for their potential endocrine-disrupting effects. The findings highlight the diversity in binding potentials across the compounds, emphasizing the need for further investigation into those demonstrating moderate interactions. According to the results, some compounds exhibited low binding potential, while others showed higher binding potential with specific receptors. Ascorbic acid demonstrated low binding potential with nearly all receptors and was mainly classified in the green category. However, its binding energy with the PR was recorded at −3.4, indicating a slight binding risk. Overall, its endocrine-disrupting effect is considered minimal. Gallic acid showed a moderate binding energy of −8.9 with the GR, while its interactions with other receptors were generally classified in the low-risk category.

This suggests that gallic acid might play a role in immune regulation or stress response mechanisms. Vanillic acid exhibited low binding potential with all receptors and was consistently classified in the green category. This indicates a very low likelihood of endocrine-disrupting effects, making it a safe phytochemical. Rosmarinic acid showed higher binding potential with PPARγ and PR receptors, which were categorized in the yellow range. This suggests it may affect lipid metabolism and hormone regulation more pronounced. Its interactions with other receptors were classified in the low-risk category. Quercetin exhibited low binding potential with all receptors and was predominantly categorized in the green category. Considering its antioxidant properties, Quercetin is regarded as a safe compound with no significant endocrine-disrupting effects. Baicalin showed moderate binding potential with specific receptors compared to the other compounds. Notably, its binding energies with GR (−8.9) and PR (−2.6) suggest that it might affect hormone regulation and stress response mechanisms, warranting further investigation. Overall, most compounds in this analysis demonstrated a low endocrine-disrupting risk profile. However, rosmarinic acid, gallic acid, and baicalin exhibited moderate binding potential with specific receptors, indicating that their effects require further detailed studies. Meanwhile, compounds like ascorbic acid, vanillic acid, and quercetin displayed a low-risk profile, positioning them as safe phytochemicals.

Although macronutrients are not directly classified as endocrine disruptors, some studies have suggested that these elements may indirectly affect endocrine functions. Mg serves as a cofactor for many enzymes involved in hormone biosynthesis and signal transmission. Mg deficiency has been associated with impaired insulin signaling and altered steroid hormone metabolism, which may enhance the effects of endocrine-disrupting chemicals (EDCs). Ca plays a crucial role in intracellular signaling pathways, particularly in the regulation of hormone secretion by thyroid and parathyroid hormones. Disruption of Ca balance can increase sensitivity to hormonal imbalances induced by EDCs. Potassium, by regulating the electrical potential of cell membranes and cellular excitability, influences the release of hormones such as insulin and aldosterone, thereby indirectly shaping physiological responses to EDCs. Furthermore, some studies suggest that the ionic environment created by macronutrients may affect the conformational state of hormone receptors or their binding affinity for ligands, potentially altering the degree to which EDCs disrupt hormone signaling pathways (Kabir et al. 2015; La Merrill et al. 2025). This information suggests that the macronutrient composition of *A. retroflexus* may influence both antimicrobial effects and potential interactions with hormone receptors.

3.6 | Molecular Docking Results: Binding Interactions of Oleuropein, Rutin, and Baicalin With Target Proteins

Table 4 provides detailed insights into the binding interactions of various compounds with the target protein 7CSW. The parameters analyzed include binding energy (ΔG), ligand efficiency (LE), fit quality (FQ), ligand lipophilic efficiency (LLE), ligand efficiency-dependent lipophilicity (LELP), estimated inhibition constant (Ki), and pIC50. These metrics collectively assess the binding strength and biological potential of the compounds. Ascorbic acid demonstrated a moderate binding energy of −5.0 kcal/mol and an LE of 0.250. However, its estimated inhibition constant (Ki = 216 μM) indicates relatively weak binding to the target protein. Gallic acid exhibited slightly better binding properties with a binding energy of −5.2 kcal/mol, an LE of 0.289, and a lower Ki value of 154 μM. Vanillic acid showed the weakest binding profile with a binding energy of −4.9 kcal/mol and an LE of 0.245. Its LLE value of −20.417 indicates poor lipophilic efficiency, and its Ki value of 256 μM further supports its limited inhibitory potential. Rosmarinic acid displayed an intermediate binding profile with a binding energy of −5.9 kcal/mol, an LE of 0.141, and a promising LLE value of 13.721. Its estimated inhibition constant (Ki = 42 μM) suggests moderate binding strength and potential biological activity. Oleuropein and rutin stood out with significantly stronger binding interactions. Oleuropein demonstrated a binding energy of −6.4 kcal/mol, an LE of 0.091, and an estimated inhibition constant.

Table 5 presents the predicted binding interactions of oleuropein, rutin, and baicalin with various amino acids and the corresponding interaction distances. This analysis provides critical insights into how these compounds interact with specific target proteins.

Significant interactions were observed with serine (SER) and methionine (MET) residues for oleuropein. Conventional and carbon–hydrogen bonds were formed with SER78 and SER75, with distances ranging from 1.82 to 3.06 Å. Additionally, alkyl interactions were identified with MET71 at 4.94 Å, and Pi-alkyl interactions with ALA53 at 5.04 Å. These interactions indicate a strong binding potential of oleuropein to the target protein (Figure S7). Rutin demonstrated a broader range of interactions with various amino acids. Conventional hydrogen bonds were observed with ALA67, GLY60, THR65, ILE57, and GLU91 at distances ranging from 1.91 to 2.87 Å. Carbon–hydrogen bonds were formed with TYR83, GLU91, and ALA80. Additionally, Pi-alkyl interactions were detected with ALA67, ARG61, and LEU79, with distances ranging from 3.35 to 5.36 Å. These findings suggest that rutin establishes multiple binding interactions with the target protein, indicating high binding affinity (Figure S8). Baicalin exhibited significant interactions with GLY50, GLN74, SER78, and ALA53 through conventional hydrogen bonds, with distances ranging from 1.86 to 2.70 Å. Carbon–hydrogen bonds were also identified with SER52 and SER75 at distances between 2.46 and 2.97 Å. These binding properties suggest that baicalin has a high binding potential to the target protein, mediated through conventional hydrogen and carbon–hydrogen bonds (Figure S9). In conclusion, the binding interactions of oleuropein, rutin, and baicalin demonstrate strong and versatile binding affinities to the target proteins. Detailed analysis of these interactions can provide valuable insights into these compounds' biological effects and potential therapeutic roles.

3.7 | Result of Network Analysis

This network analysis investigates the potential roles of various compounds in biological processes by examining their interactions with target proteins and associated biological pathways. Derived from the STRING database, the network illustrates PPIs and their impact on biological functions. The nodes (pro-

TABLE 4 | Results of binding interactions of the compounds with target 7CSW.

	Binding energy (kcal/mol)	Ligand efficiency	Fit quality (FQ)	Ligand lipophilic efficiency (LLE)	Ligand efficiency-dependent lipophilicity (LELP)	Estimated inhibition constant (Ki) (μM)	pIC_{50}
Ascorbic acid	−5.0	0.250	0.415	−3.030	−6.600	216	3.571
Gallic acid	−5.2	0.289	0.420	−6.270	−2.870	154	3.714
Vanillic acid	−4.9	0.245	0.405	−20.417	−0.980	256	3500
Rosmarinic acid	−5.9	0.141	0.490	13.721	3.060	42	4.214
Oleuropein	−6.4	0.091	0.493	−8.000	−8.750	19	4.571
Rutin	−6.9	0.095	0.524	−4.088	−17.870	8	4.929
Quercetin	−6.6	0.206	0.561	3.318	9.650	13	4.714
Baicalin	−7.7	0.154	0.655	−6.471	−7.720	2	5.500

teins) and edges (interactions) in the network highlight the significance of key proteins in regulating these processes. The analyzed network is associated with fundamental biological pathways, including cell growth, proliferation, differentiation, inflammation, oxidative stress management, metabolic regulation, and immune modulation. The network is particularly centered around key proteins such as EGFR (epidermal growth factor receptor), TNF (tumor necrosis factor), and GSK3B (glycogen synthase kinase 3 beta). These proteins are critical in cellular signaling, immune responses, and metabolic processes. EGFR is pivotal in cell growth, proliferation, and differentiation processes. Its interactions with other proteins in the network indicate its role in regulating cellular signaling pathways. TNF emerges as a critical cytokine in the regulation of inflammatory responses, and its strong connectivity with other proteins emphasizes its potential involvement in controlling inflammation and modulating immune responses. GSK3B is central to signal transduction and cellular metabolism, highlighting its essential role in these processes. Other pathways represented in the network include the regulation of oxidative stress and metabolic balance through protein–protein interactions. Proteins associated with oxidative stress demonstrate regulatory effects on redox balance and cellular protection mechanisms. Metabolic regulation involves proteins that play vital roles in energy production, lipid metabolism, and pH homeostasis, underscoring their importance in maintaining fundamental biological processes. This analysis reveals that the tight connectivity and strong interactions of central proteins within the network enable the regulation of multiple interconnected biological processes. The network interactions provide extensive insights into controlling inflammation, oxidative stress, cellular signaling, and metabolic regulation (Figure 1, 2).

This pathway analysis evaluates the potential effects of rutin and oleuropein on *P. aeruginosa*. Both compounds can influence bacterial biological pathways, significantly influencing infection control. Rutin demonstrates a notable interaction with AChE, which may indirectly affect bacterial neurotransmission systems. By interfering with quorum sensing mechanisms, rutin could inhibit biofilm formation, reducing the bacterium's capacity to establish infections and rendering it more vulnerable. This disruption of quorum sensing dynamics may also impair bacterial population coordination, limiting its pathogenicity. Conversely, oleuropein exhibits significant potential through its interactions with Interleukin 2 (IL2) and quorum sensing pathways. Its association with IL2 may influence the bacterium's recognition and response by the host immune system. Additionally, oleuropein can weaken bacterial communication and coordination by disrupting quorum-sensing mechanisms. This could restrict the bacterium's ability to form biofilms and propagate infections. The ability of oleuropein to modulate immune responses and interfere with quorum sensing highlights its potential role in bacterial infection management. Both compounds target quorum sensing pathways, impacting critical bacterial processes such as biofilm formation, secretion systems, and motility. While rutin primarily affects neurotransmission and quorum sensing, oleuropein demonstrates the potential to modulate immune responses and disrupt bacterial communication. These properties make rutin and oleuropein promising candidates for antibacterial therapies (Figure 3).

The biofilm studies revealed that compounds like quercetin, rosmarinic acid, and gallic acid significantly inhibited *P. aeruginosa* biofilm formation. These compounds are believed to exert their effects through quorum sensing inhibition, oxidative stress disruption, and destabilization of the biofilm matrix. Other compounds showed minimal to moderate biofilm inhibition and may be considered for combination therapies.

In conclusion, this study highlights the effects of specific compounds on *P. aeruginosa* biofilms, contributing to the development of new strategies for controlling antibiotic-resistant pathogens. Notably, potent compounds such as quercetin and rosmarinic acid stand out as promising candidates for preventing and treating biofilm formation.

This study conducted a network analysis to investigate biological processes related to *P. aeruginosa* infections and identify therapeutic targets associated with these processes. The analysis focused on key bacterial virulence factors, including quorum sensing, biofilm formation, flagellar motility, and secretion systems. Significant proteins identified through the network analysis included quorum-sensing regulators LasR and RhlR, the flagellar assembly regulator FleQ, the secretion system protein SecA, and the immune system–related protein IL2. Additionally, proteins

TABLE 5 | Docking of predicted interactions of docked conformations of protein.

Ligand	Amino acid	Interacting	Distance
Oleuropein	A:SER78:HG—:[001:O11	Conventional hydrogen bond	1.82
	A:SER75:HA—:[001:O10	Carbon hydrogen bond	3.06
	A:SER75:HA—:[001:O12	Carbon hydrogen bond	2.53
	A:SER75:HB1 -:[001:O10	Carbon hydrogen bond	2.90
	A:SER78:HB1 -:[001:O12	Carbon hydrogen bond	2.65
	:[001:H27 -:[001:O9	Carbon hydrogen bond	2.89
	:[001:C12 - A:MET71	Alkyl	4.94
	:[001 - A:ALA53	Pi-alkyl	5.04
Rutin	A:ALA67:HN—:[001:O6	Conventional hydrogen bond	2.38
	:[001:H17 - A:GLY60:O	Conventional hydrogen bond	1.91
	:[001:H17 - A:THR65:O	Conventional hydrogen bond	2.87
	:[001:H19 - A:ILE57:O	Conventional hydrogen bond	2.40
	:[001:H26 - B:GLU91:OE2	Conventional hydrogen bond	2.59
	B:ALA80:HA—:[001:O11	Carbon hydrogen bond	2.92
	:[001:H4 - B:TYR83:OH	Carbon hydrogen bond	2.42
	:[001:H4 - B:GLU91:OE2	Carbon hydrogen bond	2.07
	:[001 - A:ALA67	Pi-alkyl	3.34
	:[001 - A:ARG61	Pi-alkyl	5.35
	:[001 - A:ALA67	Pi-alkyl	4.59
	:[001 - B:LEU79	Pi-alkyl	5.25
	:[001 - A:ALA67	Pi-alkyl	4.86
Baicalin	B:GLY50:HN—:[001:O4	Conventional hydrogen bond	2.70
	B:GLN74:HE22 -:[001:O3	Conventional hydrogen bond	2.53
	B:SER78:HG—:[001:O3	Conventional hydrogen bond	2.23
	A:ALA53:HN—:[001:O11	Conventional hydrogen bond	2.30
	:[001:H2 - B:ILE51:O	Conventional hydrogen bond	2.08
	:[001:H11 - A:MET71:O	Conventional hydrogen bond	2.41
	:[001:H12 - A:ILE51:O	Conventional hydrogen bond	1.86
	B:SER52:HA—:[001:O5	Carbon hydrogen bond	2.80
	A:SER52:HA—:[001:O11	Carbon hydrogen bond	2.46
	A:SER75:HA—:[001:O7	Carbon hydrogen bond	2.48
	A:SER75:HB1 -:[001:O7	Carbon hydrogen bond	2.97
	A:SER75:HB1 -:[001:O8	Carbon hydrogen bond	2.65

such as PelC, which is involved in biofilm formation, and carbonic anhydrases (CA2, CA4, CA9) critical for metabolic adaptation were highlighted as key targets. Following the network analysis and literature review, oleuropein and rutin were selected as therapeutic candidates. Molecular docking studies were performed to assess their binding energies, ligand efficiencies, inhibition constants (Ki), pIC50 values, and other pharmacokinetic parameters.

The results revealed strong interactions between these compounds and their target proteins, supporting their potential as therapeutic agents. Oleuropein demonstrated a strong binding affinity for IL2, a key immune-regulatory protein. The docking analysis using the PDB structure 2B5I indicated a binding energy of −8.0 kcal/mol, LE of 0.114, and an estimated inhibition constant (Ki) of 1.920 μM. This interaction suggests that oleuropein may enhance immune responses by modulating IL2, thus supporting the host defense against bacterial infections. The role of IL2 in infection control underscores oleuropein's potential as a therapeutic agent for combating *P. aeruginosa* infections. Rutin, on the other hand, exhibited strong binding to AChE, a protein implicated in both neurological and bacterial quorum-sensing mechanisms. The docking study, utilizing the PDB structure 4EY7, revealed a binding energy of −9.6 kcal/mol, LE of 0.132,

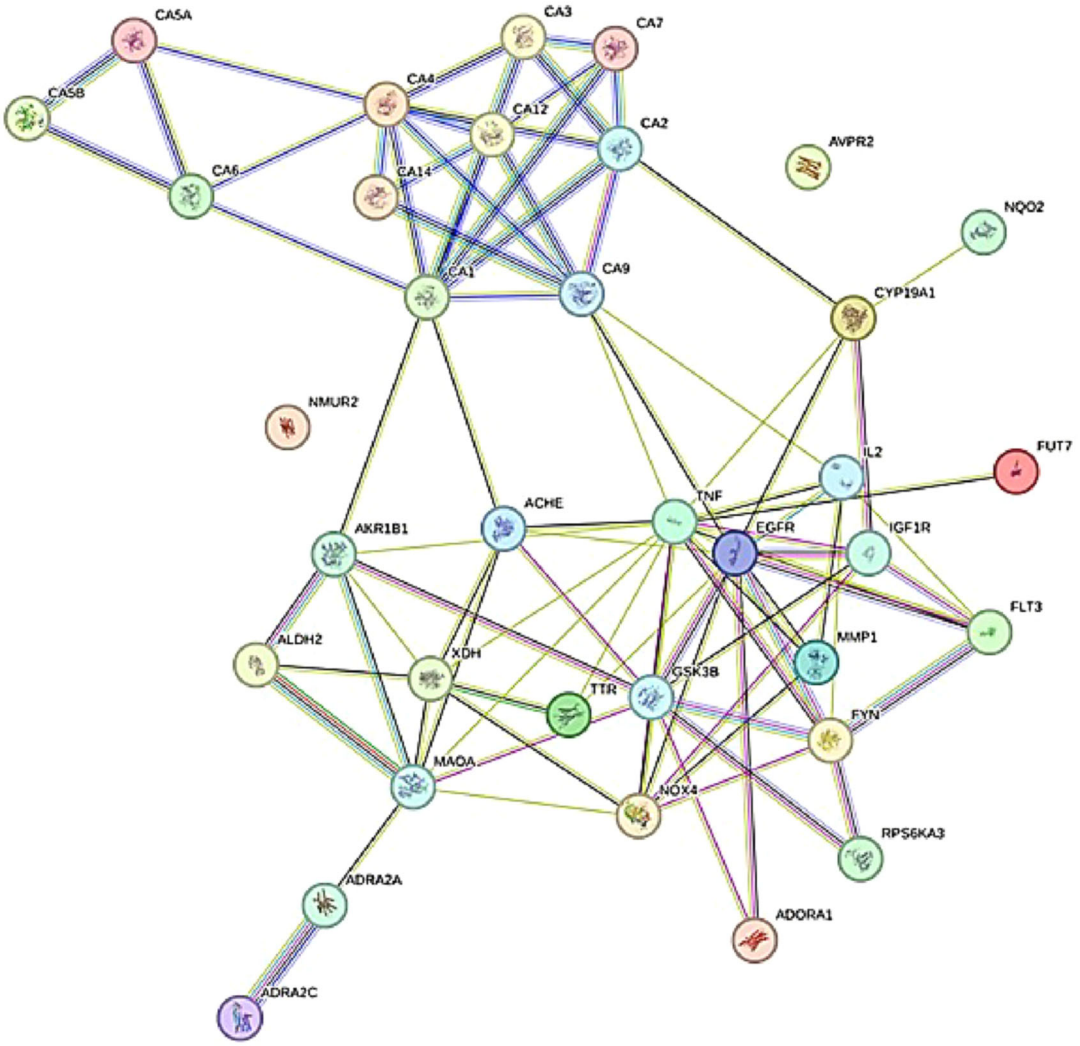

FIGURE 2 | Network analysis of protein–protein interactions based on compounds identified by HPLC analysis.

TABLE 6 | Results of binding interactions of the compounds with target protein.

	Protein	Binding energy (kcal/mol)	Ligand efficiency	Fit quality (FQ)	Ligand lipophilic efficiency (LLE)	Ligand efficiency-dependent lipophilicity (LELP)	Estimated inhibition constant (Ki) (μM)	pIC_{50}
Oleuropein	2B5I	−8.0	0.114	0.618	−10.000	−7.000	1.920	5.714
Rutin	4EY7	−9.6	0.132	0.729	−5.674	−12.860	0.038	6.857

and an estimated inhibition constant (Ki) of 0.038 μM. Rutin's potential to disrupt quorum sensing processes by targeting AChE suggests its capacity to inhibit bacterial communication and suppress virulence factor production. These findings indicate that oleuropein and rutin may disrupt critical processes in *P. aeruginosa*, including quorum sensing, flagellar motility, biofilm formation, and secretion systems. Oleuropein's modulatory effects on IL2-mediated immune responses and rutin's potential to interfere with quorum sensing highlight their therapeutic potential. Based on these results, both compounds warrant further investigation as candidates for *P. aeruginosa* infection management. Future studies should focus on validating these interactions through in vitro and in vivo experiments and optimizing these compounds for clinical applications (Table 6).

3.8 | Result of Molecular Docking: Binding Interactions of Oleuropein and Rutin With Their Target Proteins

Table 7 and Figures S10 and S11 present the binding interactions of oleuropein and rutin with their respective target proteins, detailing the types of interactions and their specific distances. The docking analysis reveals conventional hydrogen

TABLE 7 | Docking of predicted interactions of docked conformations of protein.

Ligand	Proteins	Amino acid	Interacting	Distance
Oleuropein	2B5I	D:ILE10:HN—:[001:O13	Conventional hydrogen bond	1.78
		D:ARG117:HN—:[001:O8	Conventional hydrogen bond	1.66
		D:TYR119:HN—:[001:O12	Conventional hydrogen bond	2.87
		:[001:H3 - D:GLU116:OE1	Conventional hydrogen bond	2.90
		:[001:H3 -:[001:O6	Conventional hydrogen bond	2.95
		:[001:H8 - D:GLU116:OE1	Conventional hydrogen bond	2.26
		:[001:H9 - D:THR115:O	Conventional hydrogen bond	1.81
		:[001:H29 - D:ILE10:O	Conventional hydrogen bond	2.96
		:[001:H29 - D:ALA13:O	Conventional hydrogen bond	1.99
		D:ILE118:HA—:[001:O12	Carbon hydrogen bond	2.83
		:[001:H16 - D:TYR20:OH	Carbon hydrogen bond	2.55
		:[001:H26 -:[001:O6	Carbon hydrogen bond	2.00
		:[001:H32 - D:ALA13:O	Carbon hydrogen bond	2.02
		D:PHE15 -:[001	Pi-alkyl	5.05
		D:PHE15 -:[001:C24	Pi-alkyl	5.38
		D:TYR119 -:[001:C24	Pi-alkyl	4.97
		D:PHE121 -:[001:C24	Pi-alkyl	4.17
		:[001 - D:ARG117	Pi-alkyl	3.91
Rutin	4EY7	B:ASP74:HN—:[001:O9	Conventional hydrogen bond	2.15
		B:GLY122:HN—:[001:O7	Conventional hydrogen bond	2.30
		:[001:H17 - B:TYR72:O	Conventional hydrogen bond	1.81
		:[001:H19 - B:GLN71:OE1	Conventional hydrogen bond	2.56
		:[001:H20 - B:GLU202:OE1	Conventional hydrogen bond	1.76
		:[001:H22 - B:HIS447:O	Conventional hydrogen bond	2.15
		:[001:H25 - B:ASP74:OD2	Conventional hydrogen bond	2.02
		:[001:H26 - B:ASP74:OD2	Conventional hydrogen bond	2.27
		:[001:H27 -:[001:O6	Conventional hydrogen bond	2.56
		B:THR83:HA—:[001:O14	Carbon hydrogen bond	2.74
		B:GLY126:HA2 -:[001:O5	Carbon hydrogen bond	2.43
		B:GLY448:HA1 -:[001:O12	Carbon hydrogen bond	2.64
		:[001:H2 - B:ASP74:OD2	Carbon hydrogen bond	1.47
		:[001:H8 - B:GLU202:OE1	Carbon hydrogen bond	2.94
		:[001:H8 - B:GLU202:OE2	Carbon hydrogen bond	3.05
		:[001:H5 - B:TYR337	Pi-sigma	2.77
		:[001:H7 - B:TRP86	Pi-sigma	2.20
		:[001:H23 - B:TRP86	Pi-sigma	2.68
		B:SER125:OG—:[001	Pi-lone pair	2.55
		B:SER125:OG—:[001	Pi-lone pair	2.96
		B:PHE297 -:[001	Pi-Pi T-shaped	5.82
		B:TYR341 -:[001:C1	Pi-alkyl	3.38

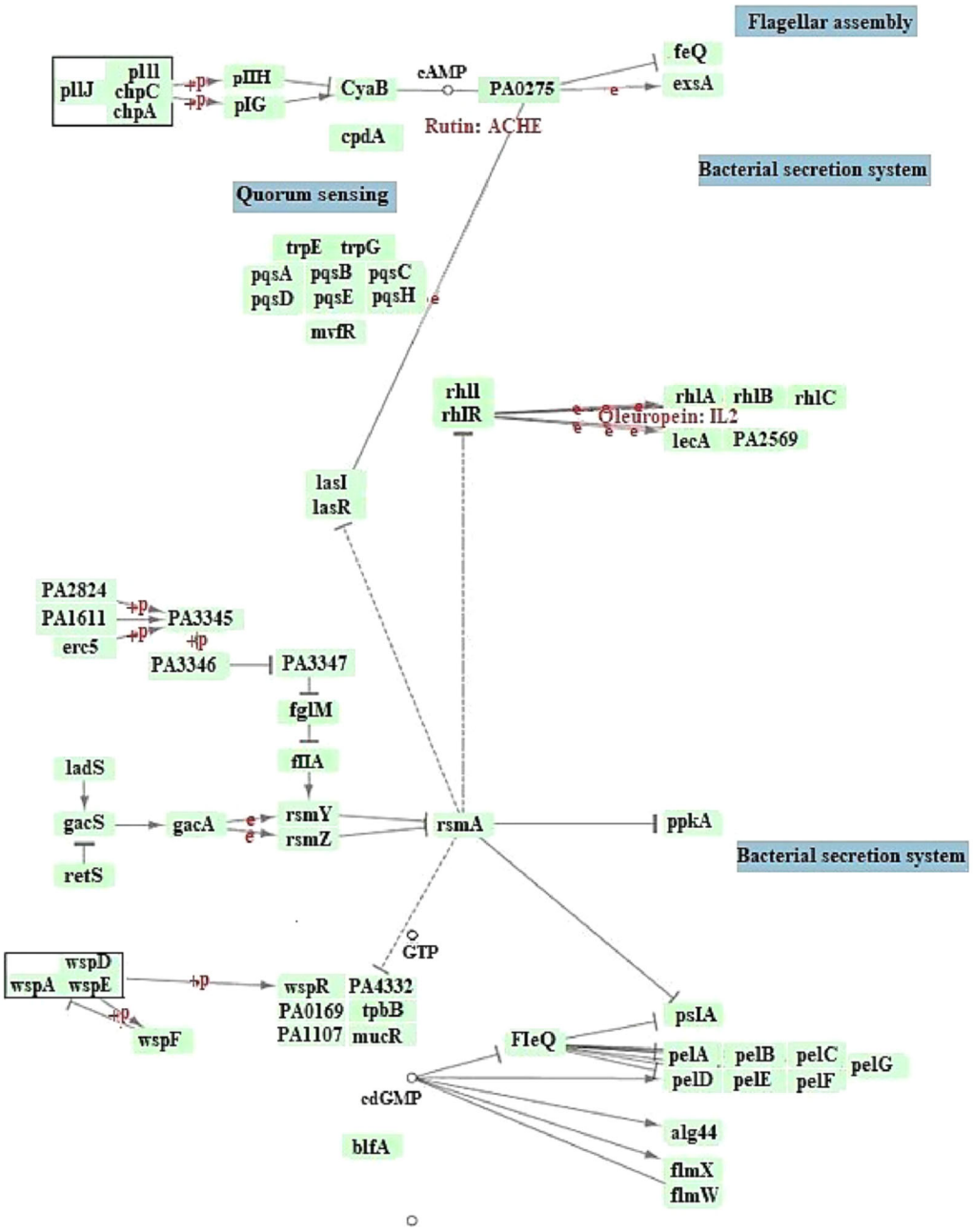

FIGURE 3 | KEGG pathway–based network analysis of rutin and oleuropein: Insights into bacterial quorum sensing and secretion systems.

bonds, carbon–hydrogen bonds, and Pi interactions, highlighting the relationships between the compounds and the amino acid residues of the target proteins.

Oleuropein demonstrated significant interactions with the 2B5I protein. It established strong conventional hydrogen bonds with amino acids such as ILE10, ARG117, TYR119, GLU116, THR115, and ALA13 in chain D. The distances of these bonds ranged from 1.66 to 2.96 Å, contributing to the stability of the binding. Additionally, carbon–hydrogen bonds were observed, particularly with residues ILE118, TYR20, and ALA13 in chain D, with bond distances ranging from 2.00 to 2.83 Å. Oleuropein also exhibited Pi-alkyl interactions with PHE15, TYR119, and PHE121, with distances varying between 3.91 and 5.38 Å. These interactions enhance oleuropein's stability and effectiveness in binding to the target protein.

Rutin displayed a wide array of binding interactions with the 4EY7 protein. It formed conventional hydrogen bonds with amino acid residues such as ASP74, GLY122, TYR72, GLN71, GLU202, HIS447, and SER125. The bond distances for these interactions ranged between 1.76 and 2.56 Å. Carbon–hydrogen bonds were also prominent, particularly with residues THR83, GLY126, and GLY448, with distances ranging from 1.47 to 3.05 Å. Moreover, rutin exhibited Pi interactions, including Pi-sigma interactions with TYR337 and TRP86 at distances of 2.20 to 2.77 Å. Pi-alkyl and Pi-lone pair interactions were also observed with TYR341 and SER125, ranging from 2.55 to 5.82 Å. These interactions significantly enhance rutin's stability and binding efficiency with its target protein.

In conclusion, oleuropein and rutin exhibit strong binding affinities and interactions with their target proteins. Their diverse

range of interactions, including conventional hydrogen bonds, carbon–hydrogen bonds, and Pi interactions, contribute to these compounds' stability and biological efficacy. These findings provide critical insights into their potential roles and mechanisms of action in biological systems.

4 | Conclusions

The extract of *A. retroflexus* exhibits antioxidant and iron chelation activities, highlighting its therapeutic potential. Rich in phytochemical constituents, the methanol extract inhibited the biofilm formation of *P. aeruginosa* while promoting biofilm formation in *S. aureus*. HPLC analysis revealed the presence of several biologically active compounds, such as ascorbic acid, gallic acid, rutin, and quercetin. Macroelement analysis suggests that *A. retroflexus* could be a valuable source of essential nutrients. Molecular docking and network analysis revealed the potential binding of key compounds like oleuropein, rutin, and baicalin with target proteins involved in cellular signaling, immune responses, and metabolic processes. These findings suggest that *A. retroflexus* compounds may play a significant role in bacterial processes, such as quorum sensing, biofilm formation, and immune regulation. *A. retroflexus* extract is a biologically active source with promising therapeutic potential. Its antioxidant, antibiofilm, and possible endocrine-disrupting properties offer valuable insights for further research and therapeutic exploration.

Author Contributions

Mehmet Aytar: conceptualization, methodology, investigation. **Emine İncilay Torunoğlu**: conceptualization, writing–review and editing, writing–original draft, formal analysis, methodology. **Erdi Can Aytar**: conceptualization, investigation, methodology, validation, software, formal analysis, writing–original draft, writing–review and editing, visualization, supervisor. **Alper Durmaz**: conceptualization, methodology, visualization, investigation. **Betül Aydın**: conceptualization, investigation, methodology, visualization. **Abidin Gümrükçüoğlu**: conceptualization, methodology, validation, funding acquisition, data curation.

Conflicts of Interest

The authors declare no conflicts of interest.

Data Availability Statement

The datasets used and/or analyzed during the current study are available from the corresponding author on reasonable request.

References

Adnan, M., M. Patel, S. Deshpande, et al. 2020. "Effect of *Adiantum philippense* Extract on Biofilm Formation, Adhesion With Its Antibacterial Activities Against Foodborne Pathogens, and Characterization of Bioactive Metabolites: An In Vitro-In Silico Approach." *Frontiers in Microbiology* 11: 823 https://doi.org/10.3389/FMICB.2020.00823/FULL.

Aldoghachi, F. E. H., U. M. N. Al-Mousawi, and F. H. Shari. 2021. "Antioxidant Activity of Rosmarinic Acid Extracted and Purified From *Mentha piperita*." *Archives of Razi Institute* 76, no. 5: 1279. https://doi.org/10.22092/ARI.2021.356072.1770.

Alfei, S., S. Catena, and F. Turrini. 2020. "Biodegradable and Biocompatible Spherical Dendrimer Nanoparticles With a Gallic Acid Shell and a Double-Acting Strong Antioxidant Activity as Potential Device to Fight Diseases From "Oxidative Stress"." *Drug Delivery and Translational Research* 10, no. 1: 259–270. https://doi.org/10.1007/S13346-019-00681-8/METRICS.

Almuhanna, Y., A. Alshalani, H. AlSudais, et al. 2024. "Antibacterial, Antibiofilm, and Wound Healing Activities of Rutin and Quercetin and Their Interaction With Gentamicin on Excision Wounds in Diabetic Mice." *Biology* 13, no. 9: 676. https://doi.org/10.3390/BIOLOGY13090676.

Amabye, T. G. 2016. "Evaluation of Physiochemical, Phytochemical, Antioxidant, and Antimicrobial Screening Parameters of *Amaranthus spinosus* Leaves." *Natural Products Chemistry & Research* 4, no. 01: 1–5. https://doi.org/10.4172/2329-6836.1000199.

Aytar, E. C. 2024. "Antioxidant and Antimicrobial Properties of *Stachys maritima* via Quantum Dots and Molecular Docking." *Chemistry & Biodiversity* 21, no. 10: e202401057. https://doi.org/10.1002/CBDV.202401057.

Aytar, E. C., E. I. Torunoglu, A. Gümrükçüoğlu, A. Durmaz, S. Al-Farraj, and M. Sillanpää. 2025. "Molecular Docking Analyses on the Chemical Profile and Antioxidant Potential of *Cakile maritima* Using GC–MS and HPLC." *Scientific Reports* 15, no. 1: 1–22. https://doi.org/10.1038/s41598-025-94887-1.

Bang, J. H., K. J. Lee, W. T. Jeong, et al. 2021. "Antioxidant Activity and Phytochemical Content of Nine *Amaranthus* Species." *Agronomy* 11, no. 6: 1032. https://doi.org/10.3390/AGRONOMY11061032/S1.

Bankar, N., L. Latta, B. Loretz, et al. 2024. "Antimicrobial and Antibiotic-Potentiating Effect of Calcium Peroxide Nanoparticles on Oral Bacterial Biofilms." *Npj Biofilms and Microbiomes* 10, no. 1: 106. https://doi.org/10.1038/s41522-024-00569-7.

Barfour, A. F., A. Y. Mensah, E. Asante-Kwatia, et al. 2021. "Antibacterial, Antibiofilm, and Efflux Pump Inhibitory Properties of the Crude Extract and Fractions From *Acacia macrostachya* Stem Bark." *Scientific World Journal* 2021, no. 1: 5381993.

Beema Shafreen, R., S. Seema, A. L. Martinez-Ayala, et al. 2019. "Binding and Potential Antibiofilm Activities of *Amaranthus* Proteins Against *Candida albicans*." *Colloids and Surfaces B: Biointerfaces* 183: 110479. https://doi.org/10.1016/J.COLSURFB.2019.110479.

Biovia. 2021. "Dassault Systèmes." Discovery Studio Visualizer, v21.1.0.20298.

Bulbul, I., L. L. Nahar, and F. Ripa. 2011. "Antibacterial, Cytotoxic and Antioxidant Activity of Chloroform, n-Hexane, and Ethyl Acetate Extract of Plant *Amaranthus spinosus*." *International Journal of PharmTech Research* 3, no. 3: 1675–1680. https://www.cabidigitallibrary.org/doi/full/10.5555/20113280527.

Caselato-Sousa, V. M., and J. Amaya-Farfán 2012. "State of Knowledge on Amaranth Grain: A Comprehensive Review." *Journal of Food Science* 77, no. 4: R93–R104. https://doi.org/10.1111/j.1750-3841.2012.02645.x.

Davis, P. 1967. *Flora of Turkey and the East Aegean Islands*. Edinburgh University Press.

Dell'Olmo, E., R. Gaglione, K. Pane, et al. 2021. "Fighting Multidrug Resistance With a Fruit Extract: Anti-Cancer and Anti-Biofilm Activities of *Acca sellowiana*." *Natural Product Research* 35, no. 10: 1686–1689. https://doi.org/10.1080/14786419.2019.1624961.

Dewanto, V., W. Xianzhong, K. K. Adom, and R. H. Liu. 2002. "Thermal Processing Enhances the Nutritional Value of Tomatoes by Increasing Total Antioxidant Activity." *Journal of Agricultural and Food Chemistry* 50, no. 10: 3010–3014. https://doi.org/10.1021/JF0115589.

Dinis, T. C. P., V. M. C. Madeira, and L. M. Almeida. 1994. "Action of Phenolic Derivatives (Acetaminophen, Salicylate, and 5-Aminosalicylate) as Inhibitors of Membrane Lipid Peroxidation and as Peroxyl Radical Scavengers." *Archives of Biochemistry and Biophysics* 315, no. 1: 161–169. https://doi.org/10.1006/ABBI.1994.1485.

Elamary, R. B., F. M. Albarakaty, and W. M. Salem. 2020. "Efficacy of *Acacia nilotica* Aqueous Extract in Treating Biofilm-Forming and Multidrug Resistant Uropathogens Isolated From Patients With UTI Syndrome." *Scientific Reports* 10: 11125. https://doi.org/10.1038/s41598-020-67732-w.

Elias, T. S., and P. A. Dykeman. 2009. *Edible Wild Plants: A North American Field Guide to Over 200 Natural Foods*. Sterling Publishing Company, Inc..

Fiorito, S., F. Epifano, R. Palmisano, S. Genovese, and V. A. Taddeo. 2017. "A Re-Investigation of the Phytochemical Composition of the Edible Herb *Amaranthus retroflexus* L." *Journal of Pharmaceutical and Biomedical Analysis* 143: 183–187. https://doi.org/10.1016/J.JPBA.2017.05.051.

Gamal, G., K. A. Abo-El-Seoud, E. Elekhnawy, and G. Attia. 2022. "Anti-Biofilm Impact of *Anabasis articulata* (Forssk) Moq. Total Methanol Extract against *Pseudomonas aeruginosa* Clinical Isolates." *Journal of Advanced Medical and Pharmaceutical Research* 3, no. 1: 29–35. https://doi.org/10.21608/JAMPR.2022.131451.1027.

Ge, C., M. Huang, D. Huang, et al. 2022. "Effect of Metal Cations on Antimicrobial Activity and Compartmentalization of Silver in *Shewanella oneidensis* MR-1 Upon Exposure to Silver Ions." *Science of the Total Environment* 838: 156401. https://doi.org/10.1016/j.scitotenv.2022.156401.

Gęgotek, A., and E. Skrzydlewska. 2023. "Ascorbic Acid as Antioxidant." *Vitamins and Hormones* 121: 247–270. https://doi.org/10.1016/BS.VH.2022.10.008.

Gümrükçüoğlu, A., A. Başoğlu, S. Kolayli, et al. 2020. "Highly Sensitive Fluorometric Method Based on Nitrogen-Doped Carbon Dotclusters for Tartrazine Determination in Cookies Samples." *Turkish Journal of Chemistry* 44, no. 1: 99–111.

Guo, W., Y. Xu, Y. Yang, et al. 2023. "Antibiofilm Effects of Oleuropein Against *Staphylococcus aureus*: An In Vitro Study." *Foods* 12, no. 23: 4301. https://doi.org/10.3390/FOODS12234301.

Hasan, I., S. N. Rahman, M. M. Islam, et al. 2021. "A *N*-acetyl-D-galactosamine-Binding Lectin From *Amaranthus gangeticus* Seeds Inhibits Biofilm Formation and Ehrlich Ascites Carcinoma Cell Growth In Vivo in Mice." *International Journal of Biological Macromolecules* 181: 928–936. https://doi.org/10.1016/J.IJBIOMAC.2021.04.052.

House, N. C., D. Puthenparampil, D. Malayil, and A. Narayanankutty. 2020. "Variation in the Polyphenol Composition, Antioxidant, and Anticancer Activity Among Different *Amaranthus* Species." *South African Journal of Botany* 135: 408–412. https://doi.org/10.1016/J.SAJB.2020.09.026.

Insuan, W., N. Hansupalak, and T. Chahomchuen. 2022. "Extraction of Curcumin From Turmeric by Ultrasonic-Assisted Extraction, Identification, and Evaluation of the Biological Activity." *Journal of Herbmed Pharmacology* 11, no. 2: 188–196.

Ivanov, M., M. Kostić, D. Stojković, and M. Soković. 2022. "Rosmarinic Acid–Modes of Antimicrobial and Antibiofilm Activities of a Common Plant Polyphenol." *South African Journal of Botany* 146: 521–527. https://doi.org/10.1016/J.SAJB.2021.11.050.

Kabir, E. R., M. S. Rahman, and I. Rahman. 2015. "A Review on Endocrine Disruptors and Their Possible Impacts on Human Health." *Environmental Toxicology and Pharmacology* 40, no. 1: 241–258. https://doi.org/10.1016/j.etap.2015.06.009.

Kırmusaoğlu, S., and H. Kaşıkçı. 2020. "Identification of Ica-Dependent Biofilm Production by *Staphylococcus aureus* Clinical Isolates and Antibiofilm Effects of Ascorbic Acid Against Biofilm Production." *Journal of Clinical Pathology* 73, no. 5: 261–266.

Kumar, A. 2024. "*Amaranthus retroflexus*: A Dual-Edged Plant With Promising Therapeutic Potential and Toxicological Concerns: A Review." *Journal of Medical Pharmaceutical and Allied Sciences* 13, no. 6: 6916–6920. https://doi.org/10.55522/jmpas.v13i6.6773.

Kumari, S., R. Elancheran, and R. Devi. 2018. "Phytochemical Screening, Antioxidant, Antityrosinase, and Antigenotoxic Potential of *Amaranthus viridis* Extract." *Indian Journal of Pharmacology* 50, no. 3: 130–138. https://doi.org/10.4103/IJP.IJP_77_18.

La Merrill, M. A., M. T. Smith, C. M. McHale, et al. 2025. "Consensus on the Key Characteristics of Metabolism Disruptors." *Nature Reviews Endocrinology* 21: 245–261. https://doi.org/10.1038/s41574-024-01059-8.

Li, W., J. Ji, X. Rui, et al. 2014. "Production of Exopolysaccharides by *Lactobacillus helveticus* MB2-1 and Its Functional Characteristics In Vitro." *LWT—Food Science and Technology* 59, no. 2: 732–739. https://doi.org/10.1016/j.lwt.2014.06.063.

Merghni, A., E. Noumi, O. Hadded, et al. 2018. "Assessment of the Antibiofilm and Antiquorum Sensing Activities of *Eucalyptus globulus* Essential Oil and Its Main Component 1, 8-cineole Against Methicillin-Resistant *Staphylococcus aureus* Strains." *Microbial Pathogenesis* 118: 74–80. https://doi.org/10.1016/j.micpath.2018.03.006.

Nazeer, S., and S. Y. Firincioglu. 2022. "Amaranth in Animal Nutrition." *Journal of Agriculture, Food, Environment and Animal Sciences* 3, no. 2: 195–211.

Nguyen, N. Y. T., N. Grelling, C. L. Wetteland, R. Rosario, and H. Liu. 2018. "Antimicrobial Activities and Mechanisms of Magnesium Oxide Nanoparticles (nMgO) Against Pathogenic Bacteria, Yeasts, and Biofilms." *Scientific Reports* 8, no. 1: 16260. https://doi.org/10.1038/s41598-018-34567-5.

Pacifico, S., B. D'Abrosca, A. Golino, et al. 2008. "Antioxidant Evaluation of Polyhydroxylated Nerolidols From Redroot Pigweed (*Amaranthus retroflexus*) Leaves." *LWT—Food Science and Technology* 41, no. 9: 1665–1671. https://doi.org/10.1016/J.LWT.2007.10.006.

Pandey, J., T. Bastola, J. Tripathi, et al. 2020. "Estimation of Total Quercetin and Rutin Content in *Malus domestica* of Nepalese Origin by HPLC Method and Determination of Their Antioxidative Activity." *Journal of Food Quality* 2020, no. 1: 8853426. https://doi.org/10.1155/2020/8853426.

POWO. 2024a. "*Amaranthus* L." Plants of the World Online, Kew Science. https://powo.science.kew.org/taxon/urn:lsid:ipni.org:names:327362-2.

POWO. 2024b. "*Amaranthus retroflexus* L." Plants of the World Online, Kew Science. https://powo.science.kew.org/taxon/urn:lsid:ipni.org:names:10698-2.

Qian, W., M. Yang, T. Wang, et al. 2020. "Antibacterial Mechanism of Vanillic Acid on Physiological, Morphological, and Biofilm Properties of Carbapenem-Resistant *Enterobacter hormaechei*." *Journal of Food Protection* 83, no. 4: 576–583. https://doi.org/10.4315/JFP-19-469.

Rastogi, A., and S. Shukla. 2013. "Amaranth: A New Millennium Crop of Nutraceutical Values." *Critical Reviews in Food Science and Nutrition* 53, no. 2: 109–125. https://doi.org/10.1080/10408398.2010.517876.

Sang, H., H. Jin, P. Song, W. Xu, and F. Wang. 2024. "Gallic Acid Exerts Antibiofilm Activity by Inhibiting Methicillin-Resistant *Staphylococcus aureus* Adhesion." *Scientific Reports* 14, no. 1: 1–11. https://doi.org/10.1038/s41598-024-68279-w.

Sărăcin, A. P., A. Biță, I. A. Sărăcin, et al. 2023. "Determination by UHPLC–UV–MS of Polyphenol Content of *Amaranthus retroflexus*." *Notulae Botanicae Horti Agrobotanici Cluj-Napoca* 51, no. 1: 13102. https://doi.org/10.15835/NBHA51113102.

Sarker, U., and S. Oba. 2020b. "Nutrients, Minerals, Pigments, Phytochemicals, and Radical Scavenging Activity in *Amaranthus blitum* Leafy Vegetables." *Scientific Reports* 10, no. 1: 3868.

Sarker, U., and S. Oba. 2020a. "Nutritional and Bioactive Constituents and Scavenging Capacity of Radicals in *Amaranthus hypochondriacus*." *Scientific Reports* 10, no. 1: 1–10. https://doi.org/10.1038/s41598-020-71714-3.

Sarker, U., S. Oba, W. F. Alsanie, and A. Gaber. 2022. "Characterization of Phytochemicals, Nutrients, and Antiradical Potential in Slim Amaranth." *Antioxidants* 11, no. 6: 1089. https://doi.org/10.3390/ANTIOX11061089.

Sarker, U., S. Oba, and M. A. Daramy. 2020. "Nutrients, Minerals, Antioxidant Pigments and Phytochemicals, and Antioxidant Capacity of the Leaves of Stem Amaranth." *Scientific Reports* 10, no. 1: 1–9. https://doi.org/10.1038/s41598-020-60252-7.

Sattar, M., F. Saeed, M. Afzaal, et al. 2024. "An Overview of the Nutritional and Therapeutic Properties of Amaranth." *International Journal of*

Food Properties 27, no. 1: 263–272. https://doi.org/10.1080/10942912.2024.2304266.

Shabani, M., Z. Jamali, D. Bayrami, and A. Salimi. 2023. "Vanillic Acid Alleviates Methamphetamine-Induced Mitochondrial Toxicity in Cardiac Mitochondria via Antioxidant Activity and Inhibition of MPT Pore Opening: An In-Vitro Study." *BMC Pharmacology and Toxicology* 24, no. 1: 1–11. https://doi.org/10.1186/S40360-023-00676-9/FIGURES/6.

Shukla, S., A. Bhargava, A. Chatterjee, J. Srivastava, N. Singh, and S. P. Singh. 2006. "Mineral Profile and Variability in Vegetable Amaranth (*Amaranthus tricolor*)." *Plant Foods for Human Nutrition* 61, no. 1: 21–26. https://doi.org/10.1007/S11130-006-0004-X.

Singhania, N., R. Kumar, Pramila, S. Bishnoi, A. B. Ray, and A. Diwan. 2024. "Bioactive Properties and Health Benefits of *Amaranthus*." In *Harvesting Food from Weeds*, edited by P. Gupta, N. Chhikara, and A. Panghal, 351–383. John Wiley & Sons. https://doi.org/10.1002/9781119793007.CH10.

Singleton, V. L., R. Orthofer, and R. M. Lamuela-Raventós. 1999. "Analysis of Total Phenols and Other Oxidation Substrates and Antioxidants by Means of Folin-Ciocalteu Reagent." *Methods in Enzymology* 299: 152–178. https://doi.org/10.1016/S0076-6879(99)99017-1.

Soriano-García, M., and I. S. Aguirre-Díaz. 2020. "Nutritional Functional Value and Therapeutic Utilization of Amaranth." In *Nutritional Value of Amaranth*, edited by V. Y. Waisundara, 101–118. IntechOpen.

Stepanović, S., D. Vuković, V. Hola, et al. 2007. "Quantification of Biofilm in Microtiter Plates: Overview of Testing Conditions and Practical Recommendations for Assessment of Biofilm Production by Staphylococci." *APMIS* 115, no. 8: 891–899.

Suwal, N., R. K. Subba, P. Paudyal, et al. 2021. "Antimicrobial and Antibiofilm Potential of *Curcuma longa* Linn. Rhizome Extract Against Biofilm Producing *Staphylococcus aureus* and *Pseudomonas aeruginosa* Isolates." *Cellular and Molecular Biology* 67, no. 1: 17–23. https://doi.org/10.14715/CMB/2021.67.1.3.

Trott, O., and A. J. Olson. 2010. "AutoDock Vina: Improving the Speed and Accuracy of Docking With a New Scoring Function, Efficient Optimization, and Multithreading." *Journal of Computational Chemistry* 31, no. 2: 455–461. https://doi.org/10.1002/JCC.21334.

Tuon, F. F., L. R. Dantas, P. H. Suss, and V. S. Tasca Ribeiro. 2022. "Pathogenesis of the Pseudomonas Aeruginosa Biofilm: A Review." *Pathogens* 11, no. 3: 300. https://doi.org/10.3390/pathogens11030300.

Wang, B., S. Shen, J. Qu, et al. 2021. "Optimizing Total Phenolic and Oleuropein of Chinese Olive (*Olea europaea*) Leaves for Enhancement of the Phenols Content and Antioxidant Activity." *Agronomy* 11, no. 4: 686. https://doi.org/10.3390/AGRONOMY11040686.

Yong, Y. Y., G. Dykes, S. M. Lee, and W. S. Choo. 2019. "Biofilm Inhibiting Activity of Betacyanins From Red Pitahaya (*Hylocereus polyrhizus*) and Red Spinach (*Amaranthus dubius*) Against *Staphylococcus aureus* and *Pseudomonas aeruginosa* Biofilms." *Journal of Applied Microbiology* 126, no. 1: 68–78. https://doi.org/10.1111/JAM.14091.

Supporting Information

Additional supporting information can be found online in the Supporting Information section.

Supporting Figures: jfds70325-sup-0001-FigureS1-S11.docx